Photoproduction of Hyperon Resonances

Jung Keun Ahn (*co-spokesperson*)
Department of Physics, Pusan National University, Pusan 609-735, Korea
email: jkahn@kaon.phys.pusan.ac.kr

and

Kenichi Imai (*co-spokesperson*)
Department of Physics, Kyoto University, Kyoto 606-8502, Japan
email: imai@nh.scphys.kyoto-u.ac.jp

August, 29, 2002

Table 1: List of Collaborators

Name	Affiliation	Position
D.S. Ahn	Dept. of Physics, Pusan National University	Master Student
J.K. Ahn	Dept. of Physics, Pusan National University	Assistant Professor
S.Y. Lee	Dept. of Physics, Pusan National University	Doctoral Student
H. Funahashi	Dept. of Physics, Kyoto University	Research Associate
K. Imai	Dept. of Physics, Kyoto University	Professor
K. Miwa	Dept. of Physics, Kyoto University	Master Student
M. Miyabe	Dept. of Physics, Kyoto University	Doctoral Student
M. Nakamura	Dept. of Physics, Kyoto University	Lecturer
M. Niiyama	Dept. of Physics, Kyoto University	Doctoral Student
M. Yosoi	Dept. of Physics, Kyoto University	Research Associate
W.C. Chang	Institute of Physics, Academia Sinica	Assistant Research Fellow
D. Oshuev	Institute of Physics, Academia Sinica	Postdoctoral Fellow
C.W. Wang	Institute of Physics, Academia Sinica	Professor
M. Fujiwara	RCNP, Osaka University	Associate Professor
T. Hotta	RCNP, Osaka University	Research Associate
H. Kohri	RCNP, Osaka University	Postdoctoral Fellow
T. Matsumura	RCNP, Osaka University	Doctoral Student
T. Mibe	RCNP, Osaka University	Doctoral Student
T. Nakano	RCNP, Osaka University	Professor
R. G.T. Zegers	RCNP, Osaka University	Postdoctoral Fellow
T. Yorita	JASRI, SPring-8	Research Associate
M. Nomachi	Dept. of Physics, Osaka University	Professor
A. Sakaguchi	Dept. of Physics, Osaka University	Associate Professor
Y. Sugaya	Dept. of Physics, Osaka University	Research Associate
M. Sumihama	Dept. of Physics, Osaka University	Doctoral Student
N. Muramatsu	Japan Atomic Energy Research Institute	Postdoctoral Fellow
T. Ishikawa	Laboratory of Nuclear Science, Tohoku University	Research Associate
H. Bhang	Dept. of Physics, Seoul National University	Professor
H. Fujimura	Dept. of Physics, Seoul National University	Postdoctoral Fellow

1 Physics Motivation

The well-established $J^p = \frac{1}{2}^- \Lambda(1405)$ hyperon competes for the distinction between an unstable $\bar{K}N$ bound state and an $L = 1$ $SU(3)$-singlet q^3 state coupled with the S-wave $\bar{K}N$ channels [1]. The world-average mass is 1406.5 ± 4.0 MeV/c^2 and its full width is 50 ± 2 MeV/c^2. Below $\bar{K}N$ threshold it decays 100% into $\Sigma\pi$ [2]. If the $\Lambda(1405)$ is a strongly bound $\bar{K}N$ state, there must exist another undetected $J^p = \frac{1}{2}^- \Lambda$ resonance lying close to the $\Lambda(1520)$. If, instead, the $\Lambda(1405)$ is the $SU(3)$-singlet uds state, it must be mass-degenerate with the $J^p = \frac{3}{2}^- \Lambda(1520)$ state. Even worse, theoretical calculations with spin-orbit interactions predict an inversion of the masses [3]. The large mass splitting must then be explained in the quark models with an anomalously large spin-orbit coupling. In the $J^p = \frac{1}{2}^-$ octet, the $\Lambda(1405)$ is, however, 130 MeV/c^2 lighter than the $J^p = \frac{1}{2}^- N^*(1535)$ even though it contains an s quark which is 100−150 MeV/c^2 heavier than the d quark. In the QCD sum rule approach, Choe *et al.*[4] predict the Λ (1405) mass to be about 1.419 GeV by choosing the $\pi^0\Sigma^0$ multiquark interpolating field. There is also a suggestion of the $\Lambda(1405)$ being a hybrid baryon $(uds)g$ where uds is in $\frac{1}{2}^+$ and g the gluon. The parity of $\Lambda(1405)$ is not yet measured experimently and its negative parity is a quark-model prediction. In this case there will be its $\frac{1}{2}^-$ hybrid partner above 300 MeV, while if the $\Lambda(1405)$ is in $\frac{1}{2}^-$, there will be as-yet-undiscovered $\frac{1}{2}^+$ states at about 1.1 GeV [5]. However, if it costs only 300 MeV for a hybrid excitation, we would have seen several hybrid states in the non-strange baryon spectrum [6].

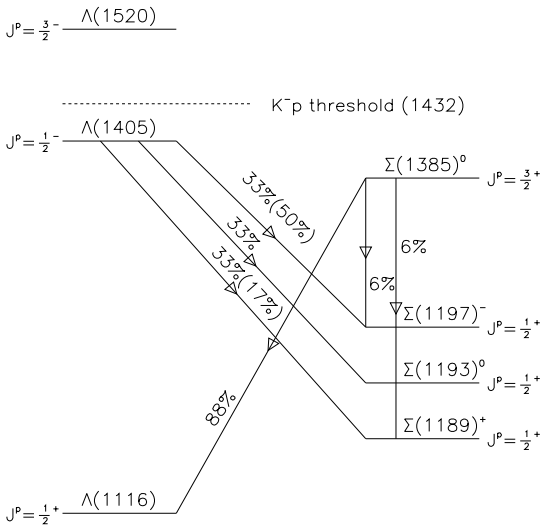

Figure 1: Shown is the decay hierarchy for $\Lambda(1405)$ and $\Sigma(1385)$.

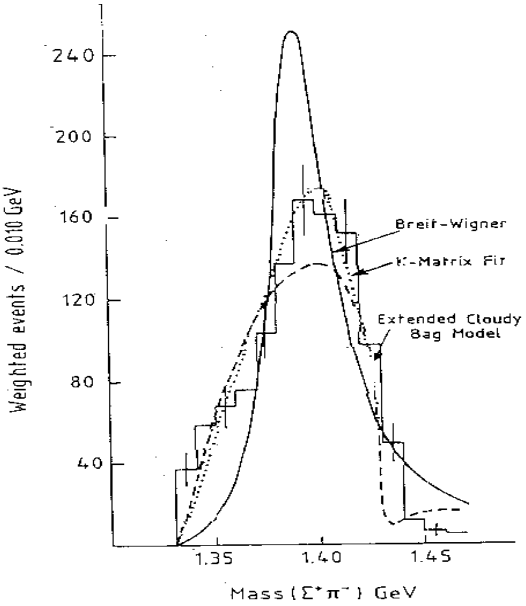

Figure 2: Hemingway's Data

Recent works of Oset *et al.* [7] predict cross sections for the lineshape of the $\Lambda(1405)$ into different channels using a chiral unitary model. In the model, the resonance $\Lambda(1405)$ is

generated dynamically from the 10 coupled channels, namely, K^-p, $\bar{K}^0n$, $\pi^0\Lambda$, $\pi^0\Sigma^0$, $\pi^+\Sigma^-$, $\pi^-\Sigma^+$, $\eta\Lambda$, $\eta\Sigma^0$, $K^+\Xi^-$, and $K^0\Xi^0$. It is interesting to see the different shapes of the three $\pi\Sigma$ channels, which can be understood in terms of the isospin decomposition. Figure 3 shows the different shape of each decay channel. Without negligible $I = 2$ contribution, they shows that

$$\begin{aligned} 3\,\frac{d\sigma}{dM}(\pi^0\Sigma^0) &\simeq \frac{d\sigma}{dM}(I=0) \\ \frac{d\sigma}{dM}(\pi^0\Sigma^0) + \frac{d\sigma}{dM}(\pi^+\Sigma^-) + \frac{d\sigma}{dM}(\pi^-\Sigma^+) &\simeq \frac{d\sigma}{dM}(I=0) + \frac{d\sigma}{dM}(I=1). \end{aligned}$$

This means that the real shape of the $\Lambda(1405)$ can be seen in either the $\pi^0\Sigma^0$ channel or the sum of the three $\pi\Sigma$ channels.

In the case of the $\Lambda(1405)$ production off nuclear targets, one can study the interaction of the $\Lambda(1405)$, propagation, and a mean-free-path in nuclear matter. Recently, Koch [9] discussed the mass shift of $\Lambda(1405)$ in nuclear matter, assuming a $\bar{K}N$ bound state. He predicts a mass shift as much as 65 MeV/c^2 for the $\Lambda(1405)$ in the normal nuclear density. Oset *et al.*[7] also stressed a possible change in mass and also in its decay width in nuclear matter. Therefore, the comparison between the $\Lambda(1405)$ and $\Sigma(1385)$ is more than important, since the $\Sigma(1385)$ is a member of the well-established SU(3) decuplet baryons, a "genuine" q^3 state.

A recent coupled-channel potential model study [8] suggests two possible interpretations of $\Lambda(1405)$, either as the 70^- three-quark state strongly coupled with $\bar{K}N$ and $\pi\Sigma$ or a $\pi\Sigma$ resonance and/or an unstable $\bar{K}N$ bound state. In the latter case, there would be a sharp resonance peak of the 70^- multiplet in the K^-p elastic cross section at laboratory momentum 170 MeV/c. Measurements of the $\pi\Sigma$ invariant mass distribution and the K^-p cross sections with higher resolution are crucial to test this model prediction.

Experimental efforts have been far behind theoretical efforts. Only two old experiments had enough statistics for a detailed analysis. Thomas *et al.* [10] reported 470 $\Sigma^+\pi^-$ and $\Sigma^-\pi^+$ events which contained no more than 50 Σ^0(1385) background events in $\pi^-p \to K^0\Sigma^\pm\pi^\mp$ at 1.69 GeV/c.

Later, Hemingway *et al.* [11] reported 766 $\Sigma^+\pi^-$ and 1106 $\Sigma^-\pi^+$ events from $K^-p \to (\Sigma\pi\pi)^+\pi^-$ at 4.2 GeV/c. In the context of the effective range approximation, these data are consistent with a Λ(1405) mass of approximately 1405 MeV/c^2 and a width of 45-55 MeV. Due to its asymmetric lineshape of the Λ(1405) mass spectrum, Hemingway's mass of 1391$\pm$1 MeV/c^2 from Breit-Wigner fit is unacceptably very poor, as shown in Fig. 2. The values quoted in Particle Data Book are $m = 1406.5 \pm 4.0$ MeV/c^2 and $\Gamma = 50 \pm 2$ MeV from Dalitz's M-matrix fit [12].

The Byer-Fenster tests on these data suggest a $J = \frac{1}{2}$ state, but cannot rule out other possibility completely. No Λ(1405) parity determination was possible because of absence of the significant polarization: Neither J nor P has yet been determined directly. The striking S-shape cusp behavior (the lineshape dropping dramatically at the approach of the $\bar{K}N$ threshold) is characteristic of S-wave coupling; the other below-threshold hyperon, the Σ(1385), has no such threshold distortion because of its $\bar{K}N$ coupling is P-wave. For the $\Lambda(1405)$, this asymmetry is the sole direct evidence that $J^p = \frac{1}{2}^-$ [1].

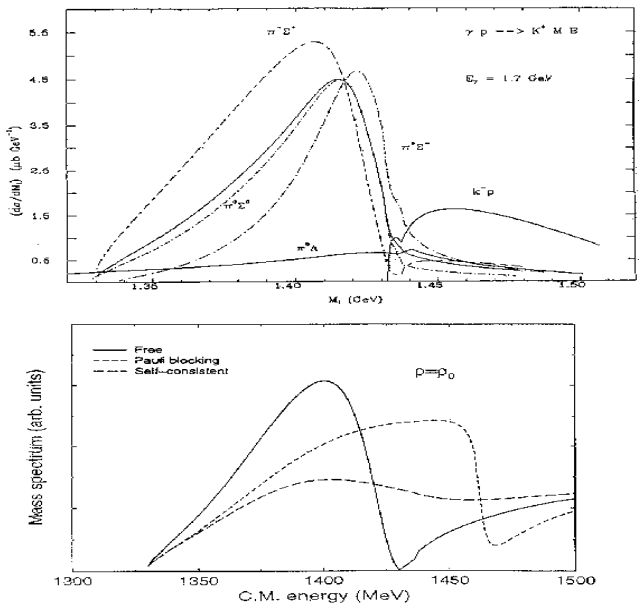

Figure 3: Invariant mass spectra for the $\Sigma^+\pi^-$, $\Sigma^-\pi^+$, and $\Sigma^0\pi^0$ channels predicted by Oset *et al.*

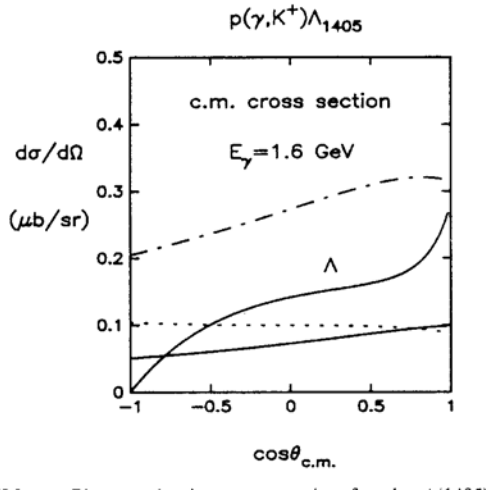

Figure 4: Differential cross section for the $p(\gamma, K^+)\Lambda(1405)$.

Therefore, the $\Lambda(1405)$ still remains as the object of sustained curiosity. Moreover, much attention is recently attracted to experimentalists for testing the reliability of χPT because it is a unique candidate for a meson-baryon bound state. Large and attractive S-wave scattering lengths of ηN and $\eta\Lambda$ make up a new η octet of $J^p = \frac{1}{2}^-$ ($N(1535)$ and $\Lambda(1670)$, respectively) associated with S-wave threshold interaction. It is also interesting to study the properties of $\Sigma(1750)(= \eta + \Sigma)$ and to search for undetected $\eta\Xi$ members.

Incorporating both crossing and duality, Williams *et al.*[13] report a comprehensive analysis of the crossing related reactions $p(\gamma, K^+)\Lambda(1405)$ and $p(K^-, \gamma)\Lambda(1405)$. They predict the $p(\gamma, K^+)\Lambda(1405)$ cross section to be sizable ($\sigma \sim 1$ b), and parity conservation leads to a model-independent suppression of the $p(\gamma, K^+)\Lambda(1405)$ polarization. They also predict differential cross sections for the $p(\gamma, K^+)\Lambda(1405)$ reaction with respect to the strength of $KN\Lambda(1405)$ coupling constant, as shown in Fig. 4.

It should be again stressed that very little experimental information is available about the $\Lambda(1405)$ properties so far. On top of that, there has been no measurements of cross sections for $p(\gamma, K^+)\Lambda(1405)$ reaction as yet. Therefore, this experiment aims at not only providing experimental information for competing theoretical predictions about the nature of the $\Lambda(1405)$, but also measuring its lineshape parameters of the $\Lambda(1405)$ and production cross sections. Considerable change in the mass and width of the $\Lambda(1405)$ in nuclear medium will strongly support its structure of meson-baryon states, mainly of a K^-p bound state. It will in turn suggest K^- condensation in neutron stars. This nature can be also tested through the ϕ photoproduction off nuclei.

2 Experimental Considerations

Since the $\Lambda(1405)$ lies just 20 MeV above the $J^p = \frac{3}{2}^-$ $\Sigma(1385)^0$ and the decay widths are 50 MeV and 36 MeV, respectively, the two particles always appear together as a combined and broad peak in a missing mass spectrum for (γ, K^+) reaction. There exist no selection rules to single out $\Lambda(1405)$ photoproduction. It therefore emphasizes the need for tagging the $\Lambda(1405)$ from its main decay branch, $\Sigma\pi$. While the $\Sigma(1385)^0$ decays 88% into $\Lambda\pi^0$ and 12% into $\Sigma^+\pi^-$ or $\Sigma^-\pi^+$, the $\Lambda(1405)$ decays almost 100% into $\Sigma^+\pi^-$, $\Sigma^0\pi^0$, or $\Sigma^-\pi^+$. The decay hierarchy for the $\Lambda(1405)$ is shown in Fig. 1.

The isoscalar $\Lambda(1405)$ will decay equally into the three charged $\Sigma\pi$ modes. However, total isospin $I = 1$ and $I = 2$ can also make up the third component of isospin zero. Without negligible $I = 2$ contribution, the cross term of $I = 0$ and $I = 1$ channels makes the $\Lambda(1405)$ decay inequally into the $\Sigma^+\pi^-$ and the $\Sigma^-\pi^+$ branches, for instance, 17% and 50%, respectively.

Taking all equal 33% decay ratios for the $\Lambda(1405)$ into account, its charged decay contributes to 6 times as large as does the $\Sigma(1385)$ decay (6% for each) in $\Sigma^-\pi^+$ and $\Sigma^+\pi^-$ states. This certainly gives a great help in getting the $\Lambda(1405)$ signal enhanced against the competing $\Sigma(1385)$ signal.

There has been no experimental data as yet published for cross section measurements of $\Lambda(1405)$ photoproduction. An old bubble chamber experiment reported the cross sections of $\sim 0.4\mu$b at 1.75 GeV for the $\gamma p \to \Sigma^+\pi^-K^+$ and the $\gamma p \to \Sigma^+\pi^-K^+$ together. A theoretical estimate of chiral unitary model gives the cross section of the order of 0.5μb (their quoted value was 5μb/GeV) [7]. Quite recently, Taylor *et al.*[14] made the cross section measurements for $\gamma p \to \Lambda\pi^0K^+$ and $\gamma p \to \Sigma^0\pi^0K^+$ reactions from thresholds to 2.4 GeV at JLab.

Supposed that all three body states come through either $\Sigma(1385)^0$ or $\Lambda(1405)$, 88% of the $\Sigma(1385)^0$ decays account for the $\gamma p \to \Lambda\pi^0K^+$ reaction, while 33% of the $\Lambda(1405)$ decays contribute to the $\gamma p \to \Sigma^0\pi^0K^+$ reaction. The $\Sigma(1385)^0$ does not decay into $\Sigma^0\pi^0$ and the $\Lambda(1405)$ decays almost 100% into $\Sigma\pi$. Therefore, our assumption is simply that there is no contribution from pure S-wave three-body reactions. It should be noted that the yield for the $\Lambda(1405) \to \Sigma^\pm\pi^\mp$ is expected to be at maximum an order of magnitude larger than that for the $\Sigma(1385) \to \Sigma^\pm\pi^\mp$. Theoretically it is also suggestive of the photon energy of $E_\gamma^{\rm lab} \sim 1.7$ GeV to be well-suited in order to suppress a P-wave contribution like the Σ^0(1385) [7].

2.1 Photon Beam

The photon beam should be highly collimated within 2 cm in diameter to prevent from directly hitting the structure of the time-projection chamber. It is needed to replace a larger-aperture collimater with the 2 cm collimator in the laser hutch, and to place the second collimator in the experimental hutch. In order to minimize e^+e^- production during the photon beam delivery, a helium bag is filled between the second collimator and the TPC.

2.2 Target

A CH_2 target is one of top candidates for photoproduction of hyperon resonances. The target length of 5 cm is equivalent to about 0.1 radiation length which is the maximum length under control. It should be noted that the 5 cm long CH_2 target contains approximately double the number of hydrogen atoms compared to the present liquid hydrogen target of the same length. For a heavier nuclear target, we choose a Cu target.

2.3 Kaon Detection and Triggers

Detecting K^+ is crucial to discriminate hyperon photoproduction processes from other huge background processes. However, the outgoing K^+ particles do not always enter the dipole spectrometer, but to a large extent they emerge in the angular region beyond the spectrometer acceptance. Since the photon energies are close to the thresholds for hyperon resonance photoproduction, the system of outgoing K^+ and produced hyperon resonance cannot be much Lorentz-boosted. This is why K^+ particles emerge all around in most cases. Based on a Monte Carlo simulation only 9% of generated events survive with K^+ particles detected at the TOF counter. This kinematical concern suggests that no specific K^+ trigger should be made. Fortunately, several charged particles are accompanied by photoproduction and decays of hyperon resonances. Therefore, it is advantageous to trigger events by requiring that there should be more than a certain number of charged particles detected at either the TOF, the TPC, or both. We are concerned with the following trigger conditions: [TPC$(\geq 1)\otimes$TOF$(\geq 1)\oplus$TPC$(\geq 2)]\otimes\overline{\mathrm{AC}}$. This trigger scheme permits us detecting K^+ in almost all scattering angles, thereby making geometrical acceptance nearly ten times larger.

2.4 Time-Projection Chamber

We have built a Time-Projection Chamber (TPC) with an active volume of 70 cm in length and 35 cm in diameter. The TPC has advantages over conventional drift chambers in several points of view: no left/right ambiguity, dE/dx measurement, less massive volume, and simple tracking in a strong homogeneous field of the existing solenoid. The TPC is composed of a single hexagonal drift volume, extending from 1.35 cm to 35 cm in radius, as shown in Fig. 5. The distance between two opposite points of the hexagonal structure is 50 cm. The inner diameter of the target cylinder is 2.5 cm and is made of G10 based substances with 2 mm thickness (less than 1% X_0). The target cylinder is 40 cm long, extending from the middle point 30 cm apart from the readout chamber through the gas-tight outer plane.

On the inner surface of the field cage are embedded 8 mm copper electrode strips in every 1 cm, while on the outer surface is made the same strips structure shifted by 5 mm. The double-sided electrodes constitute resistor chains to keep electric field constant over the whole drift volume. The target cylinder has the same structure of the electrodes. The maxium high voltage of 13.7kV keeps a uniform electric field of 200 V/cm along the drift volume. The TPC is operated with a 90/10 gas mixture Ar/CH_4 at atmospheric pressure.

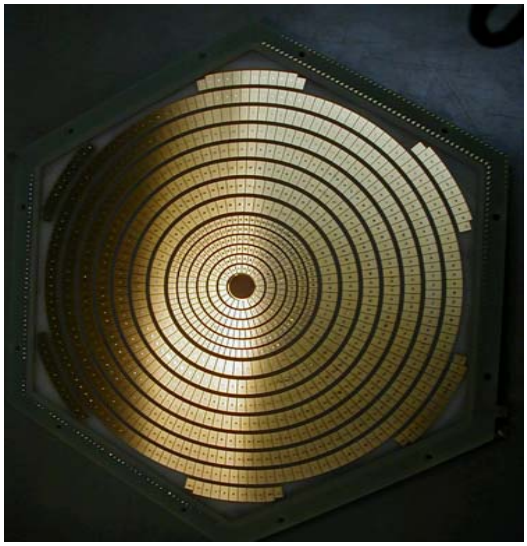
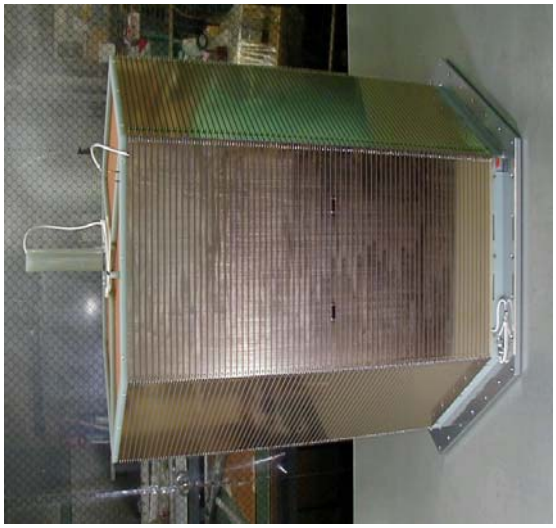

Figure 5: Left: Readout pad plane is displayed. Photon beam goes inward. Right: Photograph of the TPC.

All wires are strung along the same direction, while circular pad rows are placed radially. Anode wires will be used to measure dE/dx. The number of wires is larger than the number of pad rows in radial direction. Gain variation can be relatively easily calibrated for wire signals. There are three wire layers. The top layer is a gating grid with 2 mm wire-spacing. The gating is necessary to prevent positive ions from the avalanche. Since the drift velocity of these ions is two or three orders of magnitude slower than electrons, the positive ions will be soon full in the drift volume of the TPC, which disturb electric field. The gating wires are not used now. The second layer is a cathode grid at 0 V. The wire-spacing of the cathode grid is 2 mm, and the distance to the gating grid is 5 mm. The third layer is an anode and field wire layer, where the two wires are placed alternatively. The anode wire-spacing is 4 mm, and the anode grid is apart from the cathode grid by 4 mm.

There are two different pad configurations. The inner radial section spans from 1.3 cm to 6.9 cm, while the outer section spans from 6.9 cm to 18.4 cm. The inner section has a denser pad configuration, which consists of 7 pad rows with 4×7 mm^2 pad, 0.45 mm pitch and 2 mm row spacing. The outer section has 7 pad rows of 8×13 mm^2 pad size, 0.75 mm pitch and 4 mm row spacing. The pad-to-anode distance is 3 mm. With guard strips the region of uniform gas gain can be extended closer to the edge of a chamber.

One typical drawback of this kind of cylindrical TPC is that the spatial resolution gets worse as the polar angle of the particle track gets smaller. However, it will not matter, since a large fraction of forward particles can be tracked with the aid of the dipole spectrometer. For only a large backward angle region, we will lose the detection efficiency as the resolution gets poorer. Yet, the effective angular coverage of the TPC becomes close to $0.9 \times 4\pi$ steradian, which enhances the signals of photoproduction of the hyperon resonances by tagging K^+ at almost all lab angles. Plastic scintillation counters will surround the TPC for a timing and triggering purpose.

Table 2: Parameters of the time-projection chamber

Gas	Ar-CH_4(90%-10%)	Pressure	1 atm
Drift field E/P	200 V/cm/atm	Magnetic field	2 Tesla
Drift velocity	5 cm/μs	Lorentz angle $\omega\tau$	5.9
$\sigma_{x\,\mathrm{or}\,y}$	350 μm	σ_z	500 μm

2.5 Test-Bench Performance of the Time-Projection Chamber

Our primary goal with the TPC is to achieve excellent two-body invariant mass resolution and particle identification with a large solid angle coverage. The invariant mass resolution for symmetric two-body decays can be approximated by

$$\frac{\Delta M^2}{M^2} = \frac{2\Delta M}{M} \approx \sqrt{(\frac{4p^2 - M^2}{M^2})(\Delta\theta)^2 + 2(\frac{\Delta p}{p})^2},$$

where $p_1 = p_2 = p$, $m_1 = m_2 \sim 0$ and θ is the lab angle between $\vec{p_1}$ and $\vec{p_2}$. The resolution for asymmetric two-body decays is given in more complicated form. However, in any case the resolution is determined by two main contributions from the angular and momentum resolutions. The angular resolution is normally of the order of 1 mrad, while the momentum resolution is reportedly given at the level of 1%$\cdot p$. In this regard, the improvement of the momentum resolution is more crucial.

The momentum resolution $\Delta p/p$ can be divided into two components; $\Delta p_T/p_T$ from the p_T measurement and $\Delta\theta/\tan\theta$ from the polar angle measurement:

$$\Delta p/p = \sqrt{(\Delta p_T/p_T)^2 + (\Delta\theta/\tan\theta)^2},$$

where θ is a polar angle of the track with respect to a TPC axis. The transverse momentum resolution $\Delta p_T/p_T$ can also be written as two terms which represent an intrinsic chamber resolution $(\Delta p_T/p_T)^{IN}$ and a uncertainty due to multiple scattering $(\Delta p_T/p_T)^{MS}$, respectively:

$$\begin{aligned}
\Big\{\frac{\Delta p_T}{p_T}\Big\}^{IN} &= \frac{p_T}{0.3\cdot B(T)}\cdot\frac{\sigma_{pad}}{L_T^2}\sqrt{\frac{720}{N+4}} \\
\Big\{\frac{\Delta p_T}{p_T}\Big\}^{MS} &= \frac{1}{\sqrt{3}}\cdot\frac{0.0136}{0.3BL}\sqrt{\frac{L}{X_0}},
\end{aligned}$$

where $L_T = N\cdot L_{pad}$, the radial separation of the first and last hits on the track. N is the number of pad rows, L_{pad} the pad length, and L is the total length of the track. The factor $1/\sqrt{3}$ comes from the fact that the angle of the track is not determined by the last multiple scattering but by the overall lateral displacement with respect to the total track length.

The angular resolutions of $\Delta\theta$ and $\Delta\phi$ can also be represented as the intrinsic spatial resolution and uncertainty due to multiple scattering:

$$\Big\{\Delta\theta\Big\}^{IN} = \frac{\sigma_z}{L_z}\sqrt{\frac{12(N-1)}{N(N+1)}}, \quad \Big\{\Delta\phi\Big\}^{IN} = \frac{\sigma_{pad}}{L_T}\sqrt{\frac{192}{N+3.9}},$$

$$\text{and } \left\{\Delta\theta\right\}^{MS} = \left\{\Delta\phi\right\}^{MS} = \frac{1}{\sqrt{3}} \cdot \frac{0.0136}{\beta p}\sqrt{\frac{L}{X_0}},$$

where L_z is the length in z from the first to last hit. It turns out that we also have to improve the resolution in z direction, which depends largely on the shaping time, the number of time buckets per track and the longitudinal diffusion constant.

We have studied the intrinsic properties of the TPC, such as the drift velocity, the spatial resolutions, and the dE/dx resolution using cosmic rays. We used 8-bit 20 MHz flash ADCs with 64 channel readout channels. However, we will finally use 10-bit 40 MHz flash ADCs to read out 1055 cathode pad signals. The TPC was operated under 1.7 T high magnetic field of the solenoid. A typical cosmic ray event is displayed in Fig. 6 with an overlaid line of the reconstructed cosmic ray track. The drift velocity was measured to be 5.2 cm/μs with a 90/10 gas mixture of Ar/CH_4, as shown in Fig. 7. The position resolution along the drift direction was found to be 700 μm, which would be largely improved with 40 MHz flash ADCs. The spatial resolution on the readout plane was found to be 640 μm for the large pads and 400 μm for the small pads, respectively.

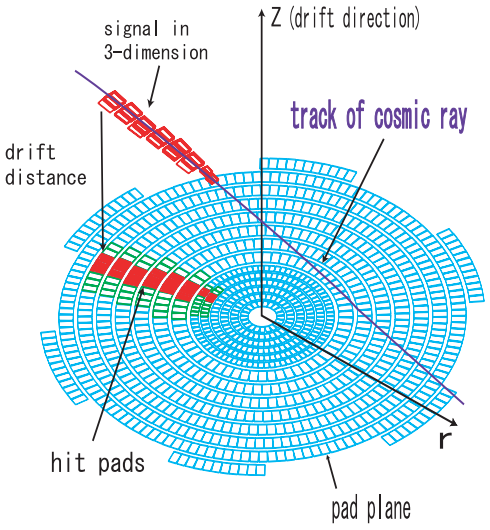

Figure 6: A typical cosmic ray event is displayed. Three-dimensionally reconstructed is the track overlaid with hit patterns.

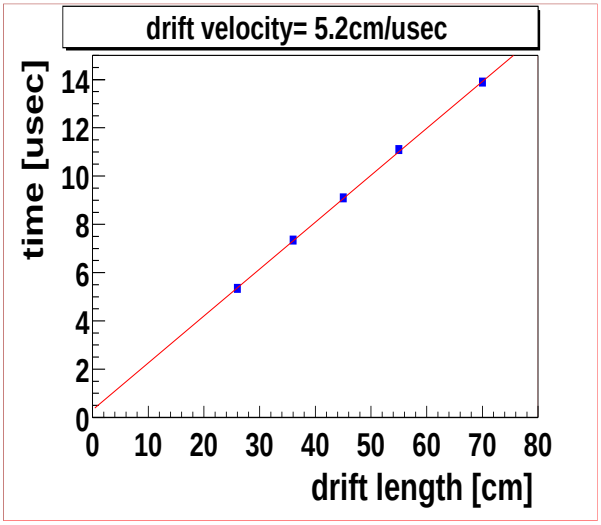

Figure 7: Drift time distribution as a function of drift length.

The spatial resolution for a single coordinate in $r-\phi$ plane is given by

$$\sigma^2 = \sigma^2_{PRF} + \sigma^2_D(L_D) + \sigma^2_W(\alpha,\psi) + \sigma^2_P(\beta),$$

where σ_{PRF} is the width of the intrinsic pad response function (PRF) due to charges induced by a single wire on the underlying pads. It mainly depends on the geometrical configuration of the sense wire and pad planes. When the pad width is approximately twice as large as the distance between the sense wire plane and the pad plane, the PRF becomes Gaussian in

good approximation and the charge is spread over two or three adjacent pads. For the 3 mm wire-pad spacing and its double pad width, the PRF is about 3 mm.

The second term σ_D^2 accounts for the transverse diffusion along the drift length.

$$\sigma_D^2(L_D) = \frac{2}{N_{\text{eff}} \cdot v_D} \frac{D_T(0)}{(1+\omega\tau)} \cdot \frac{L_D}{\cos^2\alpha},$$

where $D_T(0)$ is the transverse diffusion coefficient, and v_D the electron drift velocity.

The third term σ_W^2 represents the wire angular effect.

$$\sigma_W^2(\alpha,\psi) = \frac{d^2}{12N_{\text{eff}}^W}(\tan\alpha - \tan\psi)^2,$$

where d is the distance between two adjacent sense wires. α is the angle between the wire normal and the track projection. N_e^W is the number of charges collected over the wire gap d and is proportional to $1/(\cos\alpha \cdot \cos\lambda)$, where λ is the dip angle between the track and the wire plane. The last term σ_P^2 is due to the pad angular effect and can be written as

$$\sigma_P^2 = \frac{h^2}{12N_{\text{eff}}^P}\tan^2\beta,$$

where h is the pad height, and N_{eff}^P is the gas sample thickness along the track traversing the pad height h. β is the track angle with respect to the pad orientation. The above expression is not always true, since it diverges when β becomes too large. Instead, the PRF looses its Gaussian shape and develops a flat maximum (pad height is longer than pad width). The resolution for a longitudinal coordinate is given by

$$\sigma_z^2 = \sigma_{shaping}^2 + \frac{\Delta t^2}{12} + D_L(B)^2 L$$

where $N_0 = 90$ and $N_{\text{eff}} = 15$.

Supposed that σ_x = 0.35 mm and σ_z = 0.5mm the momentum and angular resolutions for a track leaving 13 hits at 2.0 T magnetic field are obtained to be $\{\Delta p_T/p_T\}^{IN}$ = 2.8%, $\{\Delta p_T/p_T\}^{MS}$ = 0.19%, $\{\Delta\theta\}^{IN}$ =1.1 mrad, and $\{\Delta\theta\}^{MS}$ =3.1 mrad. Reconstructing Σ decays depends on the angular resolution and momentum resolution. For a 2 GeV/c Σ, the momentum resolution is $\Delta p/p$ = 12.6%. With opening angle resolution of 50 mrad, The mean of invariant mass resolutions for the $\Lambda(1405)$ is then $\Delta M/M = \Delta M^2/(2M^2)$ =0.5%.

2.6 Reconstruction of the $\Lambda(1405) \to \Sigma\pi$ Decay

Detecting $\Sigma^{\pm}$ decays is essential to reconstruct the Λ(1405) mass. However, it requires to track the Σ particle before its decay, unless we detect π^0 and n. We then reconstruct the $\Lambda(1405) \to \Sigma\pi$ decay, hypothesizing the $\Sigma \to N\pi$ decay for a kink topology. It is therefore very important to achieve good spatial resolution in order to cope with the small-angle kink. Excellent mass resolution will enable us to observe different lineshapes of the $\Lambda(1405)$ with respect to its decay mode. The TPC meets with the need for high resolution and large acceptance.

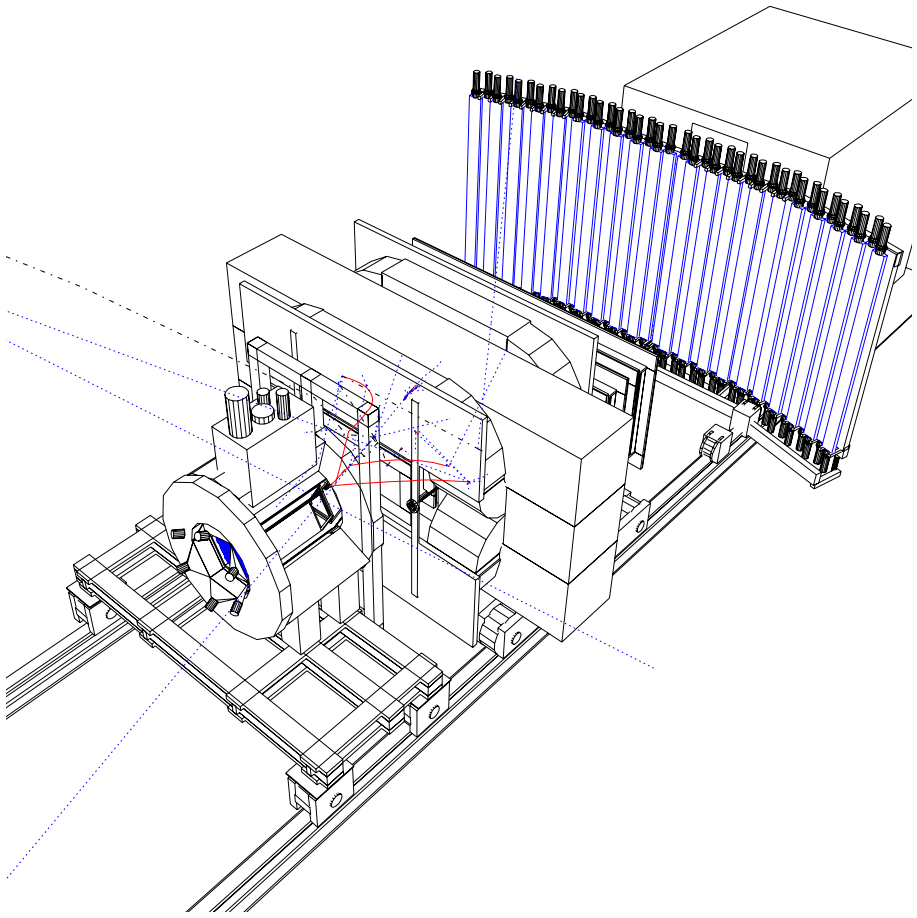

Figure 8: Layout of the LEPS spectrometer with a time-projection chamber

2.7 Count Rate

The estimate of experimental yield is based on the analysis of the SPring-8/LEPS data taken from December, 2000 through June, 2001, in order to relies not heavily on a Monte Carlo simulation. We have taken hadronic data since December, 2000, and a single bundle of each physics data set is available.

First, we attempt to select K^+ photoproduction events. Most of them are associated with photoproduction of hyperons. Figure 9 shows clear peaks for photoproduction of hyperons in the missing mass spectrum for $p(\gamma, K^+)$ reaction. The third combined peak accounts for photoproduction of the $\Lambda(1405)$ and the $\Sigma(1385)$. Since the two hyperons lies very close in mass, it is very difficult to extract the yield for the $\Lambda(1405)$ photoproduction from the single K^+ missing-mass spectrum. So we need more constraints to resolve the two hyperon peaks.

We selected the events with a K^+ and at least one pion detected simultaneously: the $\gamma p \to K^+\pi^\pm$X reaction, where X can be replaced with Σ. The missing mass spectrum for X is shown in the left panels of Fig. 10. The Σ^- hyperon peak for $\gamma p \to K^+\pi^+\Sigma^-$ reaction

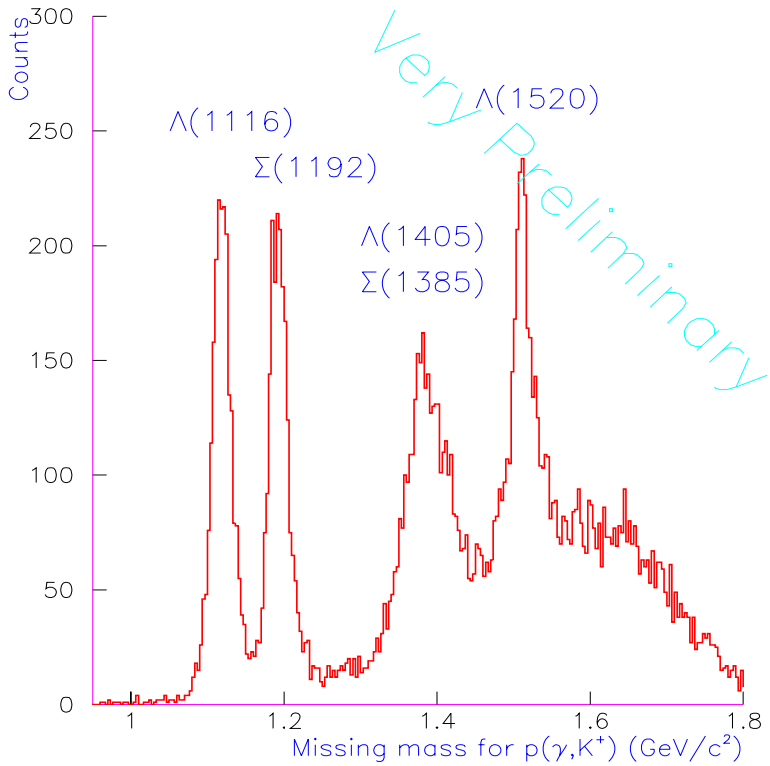

Figure 9: Missing mass spectrum for $p(\gamma, K^+)$ reaction.

appears clearly. With the calculated momentum and mass of the Σ we reconstruct $\pi\Sigma$ invariant mass in two charged channels.

The first asymmetric peak is certainly due to $\Lambda(1405)$ photoproduction, and $\Sigma(1385)$ photoproduction contribute to only one-sixth of the peak area. The $\Lambda(1520)$ also appears sharply in the $\pi\Sigma$ invariant-mass plot, since $\pi\Sigma$ and KN decay branches constitute most of its decay widths.

The number of $\Lambda(1405)$ photoproduction events in the current data set is found to be about 230 events in both channels. Therefore, the total number of $\Lambda(1405)$ particles produced in last seven calendar months can be written as

$$N_{\Lambda(1405)} = N_{\pi\Sigma K^+} \cdot R\left(\frac{\Lambda(1405)}{\Lambda(1405)+\Sigma(1385)}\right) \cdot R\left(\frac{\text{forward}\, K^+}{\pi K^+}\right) \cdot R\left(\frac{\text{all}\, K^+}{\text{forward}\, K^+}\right),$$

where $R(\frac{\Lambda(1405)}{\Lambda(1405)+\Sigma(1385)})$ denotes the ratio of $\Lambda(1405)$ to a sum of $\Lambda(1405)$ and $\Sigma(1385)$, which is set to 5/6. The second term represents the ratio of the number of K^+ particles detected to the number of both π and K^+ particles detected, and the last term accounts for acceptance of the present LEPS spectrometer. We assume a flat angular distribution for K^+ scattering angles. The second ratio and the third ratio were found to be about 23 and 10, respectively, using a Monte Carlo simulation. Therefore, over 44000 $\Lambda(1405)$ hyperons were produced from a liquid hydrogen target from last December through June.

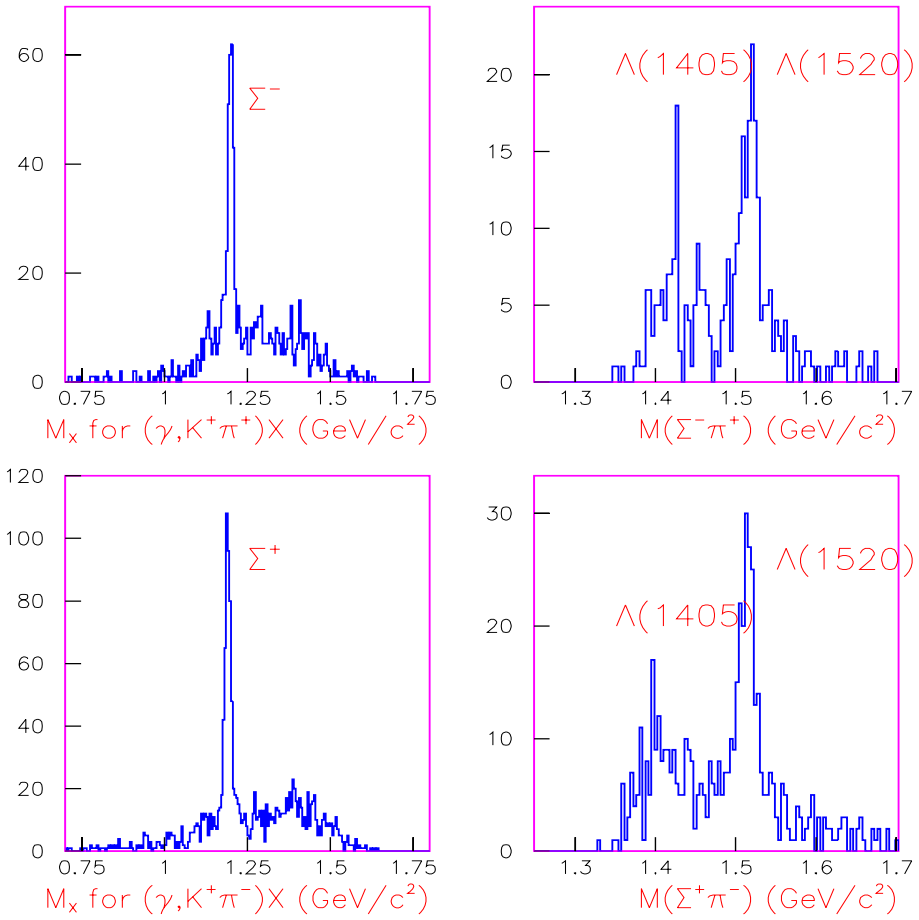

Figure 10: In the $\pi^+\Sigma^-$ (top-right) and $\pi^-\Sigma^+$ (bottom-right) invariant-mass plots the $\Lambda(1405)$ and the $\Lambda(1520)$ peaks are clearly seen. Missing mass spectra for $p(\gamma, K + \pi^+)$ reaction are shown in the left panels, where each Σ peak is dominant.

We are now interested in how many $\Lambda(1405)$ particles can be reconstructed from its characteristic $\Sigma\pi$ decay using a TPC. It is however impractical to magnetic-analyze short-lived Σ hyperon tracks of only several cm. We then reconstruct the $\Lambda(1405) \to \Sigma\pi$ decay, hypothesizing the $\Sigma \to N\pi$ decay for a kink topology. Although a TPC views particle tracks three-dimensionally, we needs to have the $r - \phi$ projected track length longer than a certain value for minimum length cutoff. To make a straight line one needs only two distinct points.

Since a π from the $\Lambda(1405)$ decay shares the same vertex point with a K^+, we already know where the line should start from. Each pad row defines one point in radius (it can have multiple points in ϕ), so we need to detect hits simply at the first pad row. However, for a conservative estimate we require that the transverse track length be longer than the center of the second pad row. This brings us a factor η_Σ, which represents the detection efficiency for shord-lived Σ hyperons using a TPC. It however heavily relies on the production and decay kinematics. If we require that either π, K^+, or both hit the TOF counter, we will be able to

select only slow Σ hyperons by kinematics. It in turn makes the total detection efficiency drop up to 1.5%. On top of that, it is worth noting that we lose 90% events when we tag K^+ only with the dipole spectrometer. Hence, the TPC is no longer a subsidiary tracking device, but a main tracker. Required that pions and K^+ going out of the dipole acceptance reach at least half a radius of the TPC, the detection efficiency for Σ, η_Σ, becomes about 8%. Summarizing, the expected yield for the $\Lambda(1405)$ photoproduction can be represented as

$$Y_{\Lambda(1405)} = N_{\Lambda(1405)} \cdot \eta_\Sigma(\vec{p}_\Sigma, \vec{p}_{K^+}, \vec{p}_\pi) \cdot \frac{L_{\mathrm{CH_2}}}{L_{\mathrm{LH_2}}} \cdot \eta_{\mathrm{rec}},$$

where the ratio $\frac{L_{\mathrm{CH_2}}}{L_{\mathrm{LH_2}}}$ accounts for the difference between CH_2 and LH_2 target lengths, which is a factor of 2. The factor η_{rec} denotes the reconstruction efficiency for the TPC data. We assume that half the total number of observed events can be reconstructed in a conservative manner. If we had performed this experiment using a TPC, we could have reconstructed 3.5×10^3 $\Lambda(1405)$ photoproduction events from December, 2000 through April, 2001. The beamtime of the five calendar months corresponds to about 210 shifts and about 1.7×10^8 online triggers. We have taken about 3.5×10^7 online triggers each month since April, 2001. Therefore, it should be stressed that we will obtain the world largest statistics for the $\Lambda(1405)$ within a couple of weeks.

3 Beam Time Request and Expected Yield

Based on the preliminary analysis results, we request 30 shifts for commissioning and 300 shifts for data-taking runs. It should be emphasized that this experiment can share the beam time with other measurements using the TPC. The photon flux should be high enough to have more than 10^6 online hadronic triggers in a day. Out of 300 shifts 200 shifts will be dedicated to the measurement with a CH_2 polyethylene target. The 5 cm long CH_2 target runs will provide us with about 3.5×10^3 $\Lambda(1405)$ events from free protons (2 protons/14g/mol $\times$ 0.95 g/cm^3 $\times$ 5 cm in Avogadro's number N_A units) and with about $1.7 \times 10^3 \times 12^\alpha$ from protons inside carbon nuclei, where the factor α accounts for A-dependence on cross sections for the $\Lambda(1405)$ photoproduction. With rest of beam time the Cu target runs will yield $0.05 \times 10^3 \times 63^\alpha$ from protons inside Cu nuclei (1 Cu nucleus/62.5g/mol $\times$ 8.96g/cm^3 $\times$ 0.15 cm in N_A units).

Table 3: Target Species and Expected Yields

Target	Beam Time (shift)	Expected Yields ($A^{0.5}$ and A^1)	
H of CH_2	200	3.5×10^3	with TPC
C of CH_2	200	5.8×10^3 — 2×10^4	with TPC
Cu	100	4×10^2 — 3×10^3	with TPC

Over three thousands $\Lambda(1405)$ events from free protons will permit very detailed analyses on its lineshapes. Moreover, the full angular coverage of the TPC enables us to make the world first measurement of differential cross sections for the $\Lambda(1405)$ photoproduction.

4 Resources Required

- Basically we need the highest intensity of photons regardless of the polarization direction. We however expect that a polarized photon beam allow the first direct measurement of the parity of the $\Lambda(1405)$. The beam energy is required to range from 1.5 GeV through 2.4 GeV.

- The dipole spectrometer is required to tag charged particles at forward angles. To obtain larger geometrical acceptance, it is needed to place the target even closer to the dipole magnet. Almost all of the pions from the $\Lambda(1405)$ decays do not exceed the threshold momentum for Cherenkov radiation traversing silica aerogel medium with $n = 1.03$. We would like to keep running the current $n = 1.03$ Cherenkov detector.

- The solenoid magnet is essential in measuring momenta of the charged particles from a target with large angles. It also helps reducing transverse diffusion of drift electrons. We will operate the solenoid at high magnetic field, 2 T.

- The time-projection chamber is a main central tracking device in this experiment.

5 Run Schedule

- In December, 2002, the solenoid magnetic field will be measured and compared with calculated results. With smaller beam collimator, the time-projection chamber will be exposed to real photons and tested with half of the readout electronics.

- By January, 2003, the time-projection chamber and its readout system will be fully prepared and tested.

- In February, 2003, the time-projection chamber will be commissioned with Compton-scattered photons during 50 shifts.

- From March, 2003, the main experiment will run with the TPC and the LEPS dipole spectrometer during 300 shifts.

- With the current setup the lineshape of the $\Lambda(1405)$ for two charged decay branchs will be thoroughly investigated until the TPC is ready.

6 Manpower Commitments

Each group possesses the manpower and expertise to complete their responsibilities in a timely manner. The participants in this proposal constitute most of the LEPS collaborators.

7 Summary

While a large body of low-energy $K^- p$ scattering data is available, the $\Lambda(1405)$ data set is very limited for more detailed analysis. The present status of the $\Lambda(1405)$ thus depends heavily on theoretical arguments. In this regard, a planned SPring-8 experiment for the $\Lambda(1405)$ photoproduction will give a clue on the nature of the $\Lambda(1405)$ and also test competing different model predictions. Under construction is a central tracking device, the TPC. It will also help us to study the properties of the $\Sigma(1385)$, $\Lambda(1520)$ and $K(892)$. We aim at performing the experiment in spring, 2003.

References

[1] R.H. Dalitz, "Note on the $\Lambda(1405)$" in C. Caro *et al. Euro. Phys. J.* **C3** 676 (1998).

[2] D.E. Groom *et al., Review of Particle Physics*, *Euro. Phys. J.* **C15**, 1 (2000).

[3] F.E. Close and R.H. Dalitz, *E. Ferrari and G. Violini (eds.), Low and Intermediate Energy Kaon-Nucleon Physics, 411*, D. Reidel Publishing Company (1981).

[4] S. Choe, *Eur. Phys. J.* **A3**, 65 (1998).

[5] O. Kittel and G.R. Farrar, *e-print* hep-ph/0010186, NYU-TH-00/09/07, 2000.

[6] S. Pakvasa and S.F. Tuan, *Phys. Lett.* **B459** 301 (1999).

[7] J.C. Nacher, E. Oset, H. Toki, A. Ramos *Phys. Lett.* **B455** 55 (1999).

[8] M. Kimura *et al., Phys. Rev.* **C62**, 015206 (2000).

[9] V. Koch, *Phys. Lett.* **B337**, 7 (1994).

[10] D.W. Thomas, A. Engler, H.E. Fisk, R.W. Kraemer *Nucl. Phys.* **B56** 15 (1973).

[11] R.J. Hemingway, *Nucl. Phys.* **B253** 742 (1985).

[12] R.H. Dalitz and A. Deloff *J. Phys. G: Nucl. Part. Phys.* **17** 289 (1991).

[13] R.A. Williams, C-R. Ji, S.R. Cotanch, *Phys. Rev.* **C43** 452 (1991).

[14] S. Taylor, "Radiative Decays of Low-Lying Excited-State Hyperons", Dissertation, University of Pittsburgh, March 2000.

[15] K. Imai *et al.* "Photoproduction of Hyperon Resonances" *Letter of Intent* at SPring-8 (1999).

[16] J.K. Ahn, "Photoproduction of the $\Lambda(1405)$" KEK Proceedings 2000-5, Workshop on Chiral Dynamics, December 9-10, Tokyo, 1999.